Fundamentals of Radar Signal Processing

About the Author

Mark A. Richards, **Ph.D.**, is an educator and consultant with over 35 years of experience in radar signal processing practice and education at the Georgia Institute of Technology, DARPA, and Lockheed Martin. He is also the co-editor of *Principles of Modern Radar: Basic Principles* and an IEEE fellow cited for "contributions in radar signal processing education."

Fundamentals of Radar Signal Processing

Mark A. Richards, Ph.D.

Third Edition

New York Chicago San Francisco
Athens London Madrid
Mexico City Milan New Delhi
Singapore Sydney Toronto

Library of Congress Control Number: 2022931805

Fundamentals of Radar Signal Processing, Third Edition

1 2 3 4 5 6 7 8 9 LCR 27 26 25 24 23 22

ISBN 978-1-260-46871-7
MHID 1-260-46871-2

This book is printed on acid-free paper.

Sponsoring Editor
Lara Zoble

Editing Supervisor
Stephen M. Smith

Production Supervisor
Lynn M. Messina

Acquisitions Coordinator
Elizabeth M. Houde

Project Manager
Rishabh Gupta, MPS Limited

Copy Editor
Surendra Shivam, MPS Limited

Proofreader
Megha Dabral, MPS Limited

Indexer
Dianna Haught

Art Director, Cover
Jeff Weeks

Composition
MPS Limited

To Theresa,
whose support made possible these books, and so much more;
and to Jessica and Benjamin,
and Amelia and Emmeline,
of whom we are so proud.

Contents

Preface

This third edition of *Fundamentals of Radar Signal Processing* (FRSP) shares with the first two editions the goal of providing an in-depth tutorial in the fundamental techniques of radar signal processing. The full spectrum of foundational methods on which virtually all modern radar systems rely is covered, including topics such as target and interference models, matched filtering, waveform design, Doppler processing, threshold detection, and measurement accuracy. Chapters or sections on tracking, adaptive array processing, and synthetic aperture imaging introduce those more advanced techniques and provide a bridge to dedicated texts.

The book is written from a digital signal processor's viewpoint. The techniques and interpretations of linear systems, filtering, sampling, Fourier analysis, and random processes are used throughout to provide a consistent and unified tutorial approach. Students should have a firm foundation in these areas to obtain the most benefit. The mathematical level is appropriate for college seniors and first-year graduate students and is leavened by extensive interpretation. Because this text concentrates on the signal processing, it does not address many other aspects of radar technology such as transmitter and receiver hardware technology or electromagnetic wave propagation. Familiarity with basic radar systems, perhaps from studying one of the books mentioned below, will help prepare the reader to get the most out of this text.

This book first came about in 2005 because I could not identify an appropriate textbook for Georgia Tech's ECE 6272, Fundamentals of Radar Signal Processing, a semester-length first-year graduate course I taught. There existed at that time a number of books on radar systems in general (e.g., Skolnik, Edde) that provided good qualitative and descriptive introductions to radar systems as a whole and could be enthusiastically recommended as first texts for anyone interested in the topic. Indeed, having worked on speech enhancement in graduate school, I read the first edition of Skolnik's classic *Introduction to Radar Systems* when I first accepted a job in radar, hoping to avoid appearing completely ignorant on my first day at the new job. (It didn't work, through no fault of Skolnik.) Some of these texts provided greater quantitative depth on basic radar systems and some signal processing topics. At the same time, a number of good texts were available on advanced topics in radar signal processing, principally synthetic aperture imaging and space-time adaptive processing. The problem, in my view, was the existence of a substantial gap between the systems books and the advanced signal processing books. Specifically, I believed the radar community lacked a current text providing a unified, modern treatment of the basic radar signal processing techniques mentioned above. The closest was probably Levanon's *Radar Principles*, which I used for early offerings of ECE 6272, but it was not comprehensive enough.

It was my hope that this book would fill that gap, and I believe it has largely been successful in doing so. However, it has now been over 16 years since the first edition was published. While new books continue to appear, particularly the excellent *Principles of*

Modern Radar series, to my surprise none has emerged that covers basic radar signal processing techniques with similar depth and breadth. In the meantime, radar technology and applications have continued to evolve, and rather rapidly. For instance, the last 10 years have seen a tremendous increase in the number of short-range continuous wave (CW) radars fielded, especially in the automotive industry. At the same time, complex new methods such as multi-input, multi-output (MIMO) processing, compressed sensing, artificial intelligence, and "deep learning" have crossed over from other application realms into advanced radar.

To continue meeting its goals, this text must also evolve. The second edition (2014) made one major addition, adding the chapter on measurement accuracy and the introduction to tracking, in addition to many more minor updates. This edition likewise has one major change. The first two editions assumed pulsed radar throughout, even though a number of the topics are also applicable to CW systems. In this edition, CW radars are now included explicitly, with an emphasis on "fast-chirp" linear frequency-modulated CW (FMCW) radars, the most common variety in current usage. Although data acquisition for pulsed and FMCW radars is very different, much of the basic processing that follows is essentially the same, a commonality that I have tried to emphasize in this edition.

Each chapter has one or two other significant updates and many small ones. Chapter 1 now includes a discussion of virtual antenna elements to set the stage for virtual arrays in Chap. 9. The discussion of Doppler shift in Chap. 2 has been simplified from that in previous editions. Also in Chap. 2, the K distribution has been added to the discussion of PDFs for describing target and clutter fluctuations.

The first portion of Chap. 3 has been significantly restructured and expanded to introduce FMCW radar, describing how range profiles are acquired and some of the range ambiguity and blind zone considerations in comparison to the pulsed case. The coherent processing interval is emphasized as a common data structure for both pulsed and FMCW, and so a common starting point for understanding subsequent processing steps.

The impact of incorporating FMCW continues in Chap. 4 with a brief discussion of CW waveforms in general before homing in on the fast-chirp linear FMCW variant of most interest. This chapter also now includes more information on mismatched filters for phase-coded waveforms and closes with a new comparison of frequency-modulated and phase-modulated waveforms.

Chapter 5 adds an introduction to the keystone transform for combatting range migration and introduces along-track interferometry (ATI) as a complement to DPCA for detecting ground movers in clutter. Chapter 6 has a new example of the effect of spiky interference on detection performance. Also new is the use of binary integration gain as an alternative way to quantify the impact of *M*-of-*N* processing.

Chapter 7 adds a brief section on the optimum combination of two noisy measurements to improve the motivation and understanding of the prediction-correction structure of most track filters. In Chap. 8, the sequence of SAR image formation algorithms has been extended to include the range migration algorithm, a workhorse in current practice, and a very basic introduction to the important emerging class of backprojection algorithms.

Chapter 9 now introduces the idea of virtual arrays (VAs), essential to the understanding of MIMO array systems. While MIMO processing itself is beyond the scope of this text, the discussion of VAs provides a base for its study in more specialized references. Also, both phase and time delay steering of arrays are now discussed and compared explicitly. The two appendices are largely unchanged except for the addition of the K distribution to the PDFs, discussed in App. A. Finally, some additional homework problems have been added to most chapters to improve the book's usefulness as an academic text.

Throughout the text, I once more attempt to do a better job of identifying and bringing out common themes that arise again and again in radar signal processing, if sometimes in

disguise. These include phase history, coherent integration, matched filtering, integration and processing gain, and maximum likelihood estimation.

Several ancillary FRSP materials are available from the publisher. An errata list and a collection of MATLAB® demonstrations of various fundamental radar signal processing operations are available to all readers at www.mhprofessional.com/Richards3e. For instructors of classes using this book as a text, there is a solution manual for the end-of-chapter problems and a collection of MATLAB® mini-projects with sample solutions. While not directly related to FRSP, a series of technical memos on additional radar signal processing topics can be found by the reader at the author's website www.radarsp.com.

A one-semester course in radar signal processing can cover Chaps. 1 through 7, perhaps skipping some of the later sections of Chaps. 2 and 3 for time savings. Such a course provides a solid foundation for more advanced work in detection theory, adaptive array processing, synthetic aperture imaging, and more advanced radar concepts such as passive and bistatic systems. A quarter-length course could cover Chaps. 1 through 5 and the non-CFAR portion of Chap. 6 reasonably thoroughly. In either case, a firm background in basic continuous and discrete signal processing and an introductory exposure to random variables and processes are advisable.

I have tried in this edition to eliminate all known errors in the second edition, but because there is significant new material, there are likely new errors. I invite readers to help me keep the errata sheet up to date by sending any and all errors they find to me at mrichards@ieee.org.

Mark A. Richards, Ph.D.
January 2022

Acknowledgments

I remain indebted to many colleagues and students who have helped me over the years to learn this material and how to write and teach it. A few on whom I have relied the most, and who have in particular helped me with topics in this edition, merit special mention. Dr. Byron Keel continued to share his expertise in waveforms and CFAR, especially in comparing frequency- and phase-modulated waveforms. Dr. Greg Coxson and Jon Russo helped with the current state of the art in optimum phase codes. Samuel Piper helped me both directly and through his own publications with the new CW radar material. Dr. James Sangston helped me develop the mathematics and an example of detection in spiky clutter. Dr. Gregory Showman helped me to understand the SAR range migration and backprojection algorithms, providing the base for the RMA derivation and several simulation examples that appear in Chap. 8. Prof. Nadav Levanon of Tel Aviv University has exchanged many materials and ideas with me for some years now, especially regarding waveforms, Doppler processing, and radar education. I am grateful to each of them for their knowledge, assistance, and friendship both in preparing this edition and throughout my career.

Selected Symbols

The following definitions and relations between symbols are used throughout this text except as otherwise specifically noted. Some symbols, for example θ, have more than one usage; their meaning is generally clear from the context.

$*$	Convolution operator
$\otimes$	Kronecker product operator
$\odot$	Hadamard product operator
(x)	Continuous variable x
$[x]$	Discrete variable x
$((\cdot))_x$	Modulo x
$\mathbf{0}_N$, $\mathbf{1}_N$	N-element vector of zeroes, ones
$\sim$	"Is distributed as"
$\mathbf{x}$	Vector variable
$\mathbf{X}$	Matrix variable
x^*	Complex conjugate of x
$\mathbf{x}^H$, $\mathbf{X}^H$	Hermitian transpose of vector or matrix $\mathbf{x}$, $\mathbf{X}$
$\mathbf{x}^T$, $\mathbf{X}^T$	Transpose of vector or matrix $\mathbf{x}$, $\mathbf{X}$
α_q	Clutter temporal fluctuation vector
α	Threshold multiplier, cell-averaging CFAR
α_{GO}	Threshold multiplier, "greatest-of" CFAR
$\alpha_{\log}$	Threshold multiplier, log CFAR
α_{OS}	Threshold multiplier, order statistic CFAR
α_{SO}	Threshold multiplier, "smallest-of" CFAR
β	Bandwidth
β_3	3-dB bandwidth
β_D	Doppler bandwidth
β_{MLC}	Mainlobe clutter bandwidth
β_n	Noise-equivalent receiver bandwidth
β_{nn}	Null-to-null bandwidth
β_r	Rayleigh bandwidth
β_{rms}	Root-mean-square bandwidth
β_x, β_y, β_z	Spatial frequency bandwidth in x, y, and z dimensions
γ	Interferogram coherence; Q channel DC offset
γ_c	Clutter ridge slope
Γ	Tracking index; gamma function
δ	Grazing angle

$\delta[\cdot]$	Discrete-variable impulse function
$\delta\theta$	Target angle relative to boresight
$\delta_D(\cdot)$	Continuous-variable Dirac impulse ("delta") function
δR	Range error
δR_s	Range bin spacing
δt	Differential delay
$\Delta\theta$	Angular resolution; lobing antenna squint
$\Delta\psi$	Change in squint angle
ΔCR	Cross-range resolution
ΔF	Frequency step size
ΔF_D	Doppler frequency resolution
Δh	Height displacement
ΔR	Range resolution
ΔR_b	Range relative to central reference point
ΔR_c	Range curvature
ΔR_w	Range walk
Δt	Time resolution
Δt_b	Time relative to central reference point delay
ε	I/Q amplitude mismatch; mismatch error
$\varepsilon_{\Delta/\Sigma}$	Error in lobing antenna ratio voltage $v_{\Sigma/\Delta}$
ζ	Baseband reflectivity amplitude ($\zeta \geq 0$)
$\overline{\zeta}$	Non-baseband reflectivity amplitude ($\overline{\zeta} \geq 0$)
η	Volume reflectivity
θ	Azimuth angle; phase; baseband transmitted signal phase
$\theta(t)$	Phase modulation of waveform
θ_3	3-dB beamwidth
θ_{az}	Azimuth beamwidth
θ_{el}	Elevation beamwidth
θ_{nn}	Null-to-null azimuth beamwidth
θ_R	Rayleigh beamwidth
θ_{SAR}	Effective beamwidth of synthetic aperture radar
Θ	Parameter to be estimated
$\boldsymbol{\Theta}$	Parameter vector to be estimated
$\hat{\Theta}$	Estimate of Θ
$\hat{\boldsymbol{\Theta}}$	Estimate of $\boldsymbol{\Theta}$
κ	I channel DC offset; Doppler spectrum oversampling factor
$\ell(a\|b)$	Likelihood function for parameter a given data b
λ	Wavelength; eigenvalue
Λ	Likelihood ratio
λ_t	Transmitted signal wavelength
$\rho = \zeta\exp(j\psi)$ $= \rho_{\mathrm{I}} + j\rho_{\mathrm{Q}}$	Complex baseband reflectivity
ρ_{I}	Baseband reflectivity in-phase (I) component
ρ_{Q}	Baseband reflectivity quadrature-phase (Q) component
ρ_f, ρ_{fg}	Normalized autocorrelation of function f, or cross-correlation of functions f and g
ρ'	Effective baseband complex reflectivity
$\tilde{\rho}$	Cross-range averaged effective baseband complex reflectivity
$\tilde{\mathrm{P}}$	Range spatial spectrum (Fourier transform of $\tilde{\rho}$)

$\sigma = \lvert\rho\rvert^2 = \zeta^2$	Radar cross section (RCS)
σ^0	Area reflectivity
σ_h	Surface roughness
σ_x^2	Variance of random variable x
$\sigma_{\hat{\Theta}}$	Precision of estimate of Θ
ϕ	Elevation angle; phase
ϕ_3	3-dB elevation beamwidth
ϕ_{fg}	Interferometric phase difference
ϕ_n	Subpulse (chip) phase in phase-coded waveform
ϕ_{nn}	Null-to-null elevation beamwidth
τ	Pulse length
τ_c	Subpulse length in phase-coded waveform
φ	Baseband phase
χ	Signal-to-noise ratio
χ_1	Single sample signal-to-noise ratio
χ_N	N-sample signal-to-noise ratio
χ_{out}	Output signal-to-noise ratio
χ_∞	Signal-to-noise ratio with perfect noise level estimate
χ_Σ	Lobing antenna sum channel signal-to-noise ratio
ψ	Baseband reflectivity phase; squint angle; cone angle
ω	Normalized frequency (radians per sample)
ω_D	Normalized Doppler frequency shift (radians per sample)
ω_s	Sampling interval in normalized frequency ω (samples per radian)
Ω	Frequency (radians per second); solid angle
Ω_θ	Azimuth rotation rate (radians per second)
Ω_D	Doppler frequency shift (radians per second)
Ω_{diff}	Doppler frequency mismatch (radians per second)
Ω_i	Matched Doppler frequency shift (radians per second)
Ω_t	Transmitted or carrier frequency (radians per second)
Υ	Sufficient statistic
a	Baseband transmitted signal amplitude
$\mathbf{a}_s(\theta)$	Spatial steering vector
$\mathbf{a}_t(\theta)$	Temporal steering vector
$A(t, F_D)$, $\hat{A}(t, F_D)$	Ambiguity function, complex ambiguity function
A, $\hat{A}$, $\overline{A}$	Signal amplitude
A_e	Effective antenna aperture size
$\mathbf{A}_q$	Covariance matrix of clutter temporal fluctuations
A_n	Complex amplitude of subpulse in phase-coded waveform
$AF(\theta)$, $AF(\theta, \phi)$	Phased array antenna array factor
B	Number of bits; interferometric baseline
B_N	Length of Barker phase code
c	Speed of electromagnetic wave propagation
$\mathbf{c}_q$	Clutter space-time steering vector for patch q
CA	Clutter attenuation
$\text{CN}(a, b)$	Complex normal (Gaussian) distribution with mean a and variance b
$CRLB$	Cramèr-Rao lower bound
$C_x(\cdot)$	Characteristic function of random variable x; centroid of signal x
d	Phased array element spacing
$d_g(\cdot)$	Group delay function

d_M	Mahalanobis distance
d_{pc}	Phase center spacing
D	Antenna aperture size
D_{az}	Antenna size, azimuth dimension
D_{el}	Antenna size, elevation dimension
D_{SAR}	Synthetic aperture size
DOF	Degrees of freedom
DR	Dynamic range
D_x, D_y, D_z	Antenna aperture size in x, y, or z dimension
$\mathbf{e}$	Eigenvector
E, E_x	Energy; energy in signal x
$\mathbf{E}\{\cdot\}$	Expected value
$E(\theta, \phi)$	Electric field amplitude
$E_{el}(\theta)$, $E_{el}(\theta, \phi)$	Phased array antenna element pattern
f	Normalized frequency (cycles per sample)
$\tilde{f}$	Quantized version of a function f
f_D	Normalized Doppler frequency shift (cycles per sample)
f_{Dt}	Target normalized Doppler frequency shift (cycles per sample)
f_θ	Normalized spatial frequency (cycles per sample)
F	Frequency (hertz); Fourier transform of a function f
$\mathbf{F}$	Fourier transform operator; track filter state transition matrix
F_θ	Spatial frequency (cycles per meter)
F_b	Beat frequency; blind Doppler frequency (hertz)
$F_{b\max}$	Maximum beat frequency (hertz)
$F_{b\min}$	Minimum beat frequency (hertz)
F_{bs}	Blind Doppler frequency using staggered PRIs
F_c	Corner frequency (hertz)
F_D	Doppler frequency shift (hertz)
F_{Da}	Apparent Doppler frequency (hertz)
F_{diff}	Doppler frequency mismatch (hertz)
F_{Dua}	Unambiguous Doppler frequency interval (hertz)
F_g	Greatest common divisor of a set of staggered PRFs
F_i	Instantaneous frequency (hertz)
F_n	Noise figure
F_r	Received frequency (hertz)
F_s	Sampling frequency (samples per second)
F_t	Transmitted or carrier frequency (hertz)
F_{us}	Unstaggered blind Doppler frequency
$\mathbf{g}$, $\mathbf{G}$	Tracking process noise gain
G	Antenna power gain
G_{nc}	Noncoherent integration gain
G_s	Maximum receiver gain
G_{sp}	Signal processing gain
h	Height
$\mathbf{h}$	Filter weight vector; beamformer weight vector
$\mathbf{h}$, $\mathbf{H}$	Tracking observation matrix
$h(t)$	Impulse response (continuous time)
$h[n]$	Impulse response (discrete time)
$h_p(t)$	Matched filter impulse response for individual pulse
H_0	Null hypothesis (interference only)
H_1	Non-null hypothesis (target plus interference)

$H(f)$, $H(F)$, $H(\omega)$, $H(\Omega)$	Frequency response in various units
$H(z)$	Discrete-time system function
$H_N(z)$	System function of N-pulse canceller
$H_{N,P}(F)$	Frequency response of N-pulse canceller with P staggered PRFs
I; I	In-phase channel; in-phase channel signal; interference power; improvement factor
I_{opt}	Improvement factor for matched filter
$I_N(\cdot)$	Modified Bessel function of the first kind and order N
$\mathbf{I}_N$	Nth-order identity matrix
$I(\cdot, \cdot)$	Incomplete gamma function
$\mathbf{I}(\cdot)$	Fisher information matrix
$J_n(t)$	Jammer signal
$\mathbf{J}$	Jammer signal sample vector
k_p	Stagger ratio
$k_{\Delta/\Sigma}$	Lobing antenna Δ/Σ error slope
$k_\theta = -\tilde{k}_\theta$	Normalized spatial frequency (cycles per sample)
K, $\mathbf{k}$, $\mathbf{K}$	Tracking filter gain; Kalman filter gain (symbol varies with dimensionality)
K	Spatial frequency (radians per meter); DFT, IDFT, FFT, or IFFT size; normalized quantizer step size
K_R	Range spatial frequency (radians per meter)
K_u	Cross-range spatial frequency (radians per meter)
K_x, K_y, K_z	Spatial frequency in x, y, or z dimension (radians per meter)
K_θ	Spatial frequency corresponding to AOA θ (radians per meter)
k_θ	Normalized spatial frequency corresponding to AOA θ (radians per sample)
L	Number of fast-time samples per pulse
L_a	Atmospheric loss factor
L_d	Target depth as viewed from the radar
L_s	System loss factors; synthetic aperture radar swath length
L_{SIR}	Signal-to-interference ratio loss
L_w	Target width as viewed from the radar
LPG	Loss in processing gain
M	Number of slow-time samples per coherent processing interval
$\mathbf{M}$	Tracking mean-square error estimate matrix
M_{DD}	Minimum detectable Doppler shift
M_{DD+}, M_{DD-}	Minimum detectable positive, negative Doppler shift
M_{opt}	Optimum value of M in "M of N" detection rule
M_s	DPCA time slip
n_P	Matched filter output noise power
N	Noise power; number of phase code chips; number of phase centers
N(a, b)	Normal (Gaussian) distribution with mean a and variance b
N_γ	Number of spotlight SAR radial slices
N_R	Number of spotlight SAR range samples
N_{spot}	Number of spotlight SAR images per unit time
$p_x(\cdot)$	Probability density function for a random variable x
$P_x(\cdot)$	Cumulative density function for a random variable x
P	Power; degrees of freedom in space-time snapshot
$P(\theta, \phi)$	Antenna one-way power pattern
$P_\theta(\theta)$	Azimuth one-way antenna power pattern
$P_\phi(\phi)$	Elevation one-way antenna power pattern

P_b	Backscattered power
P_{BD}	Binary integrated probability of detection
P_{BFA}	Binary integrated probability of false alarm
P_{CD}	Cumulative probability of detection
P_{CFA}	Cumulative probability of false alarm
P_D	Probability of detection
P_{FA}	Probability of false alarm
P_M	Probability of miss
P_o	Output power
P_r	Received power; relative power of I/Q mismatch image
$\Pr\{\cdot\}$	Probability of argument occurring
P_t	Transmitted power
PL	Processing loss
PRF	Pulse repetition frequency (pulses per second)
q	Quantizer step size
Q, Q	Quadrature channel
Q	Power density; quadrature channel signal
Q_b	Backscattered power density
Q_k	Quadrature component, sample k
Q_M	Marcum Q function
Q_t	Transmitted power density
R, R_0	Range
R_a	Apparent range
R_b	Blind range
RI	Repetition interval
$R_{\max}$	Maximum range
$R_{\min}$	Minimum range
RR	Repetition rate
R_{ua}	Unambiguous range
R_{uas}	Unambiguous range using staggered PRIs
R_w	Range window; range swath
s_A	Autocorrelation of phase code complex amplitude sequence
s_f	Autocorrelation of a function or random signal f
s_{fg}	Cross-correlation of functions or random signals f and g
$s_p(t)$	Output of filter matched to single pulse in pulse train waveform
$\mathbf{S}$	Polarization scattering matrix
$S_f(\omega)$	Power spectrum of a function or random signal f
$S_{fg}(\omega)$	Cross-power spectrum of functions or random signals f and g
$\mathbf{S}_\mathbf{x}$	Covariance matrix for a random vector $\mathbf{x}$
$\tilde{\mathbf{S}}_x$	Transformed covariance matrix
$\hat{\mathbf{S}}_x$	Estimated covariance matrix
SIR	Signal-to-interference ratio
$SQNR$	Signal-to-quantization noise ratio
t, t_0	Time
$\mathbf{t}$	Target model vector
$\tilde{\mathbf{t}}$	Transformed target model vector
T	Pulse or sweep repetition interval; detection threshold; track measurement update interval
$\mathbf{T}$	Transformation matrix
T'	Equivalent receiver temperature; detection threshold

T_θ	Sampling interval in θ
T_a	Aperture time
T_{avg}	Average PRI of a set of staggered PRFs
T_M	Time of matched filter output peak
T_p	pth PRI in set of staggered PRFs
T_s	Fast-time sampling interval; sampling interval in $s = \sin\theta$
T_{tot}	Sum of PRIs corresponding to staggered set of PRFs
T_w	Time corresponding to swath width
u	Along-track coordinate of synthetic aperture radar platform
u, $\mathbf{u}$	Tracking process noise
$UDSF$	Usable Doppler space fraction
$\text{var}(x)$	Variance of random variable x
v	Platform velocity
$v_{\Sigma'} v_\Delta$	Sum and difference lobing voltages
$v_{\Sigma/\Delta}$	Lobing antenna ratio voltage
v_a	Apparent velocity
v_b	Blind speed
v_{bs}	Blind speed using staggered PRIs
v_L, v_R	Left and right lobing antenna voltages
v_{ua}	Unambiguous velocity interval
w, $\mathbf{w}$	Tracking measurement noise
$\mathbf{w}_f$	Temporal weight vector
$\mathbf{w}_\theta$	Spatial weight vector
(x, y, z)	Position in Cartesian coordinates
$(\dot{x}, \dot{y}, \dot{z})$	Velocity in Cartesian coordinates
$\overline{x}$	Mean of random variable x
$\hat{x}$	Estimated value of random variable x
$x = x_{\text{I}} + j\, x_{\text{Q}}$	Transmitted signal, baseband
$\overline{x} = \overline{x}_1 + j\overline{x}_Q$	Transmitted signal, non-baseband
x_P	Along-track coordinate of synthetic aperture radar scatterer
$x_p(t)$	Subpulse of phase-coded waveform; single pulse of pulse train waveform
$y = y_{\text{I}} + jy_{\text{Q}}$	Received signal, baseband
$\mathbf{y}$	Baseband received signal sample vector
$\tilde{\mathbf{y}}$	Transformed baseband received signal sample vector
$\overline{y} = \overline{y}_I + j\overline{y}_{\text{Q}}$	Received signal, non-baseband
$y[l, m, n]$	Datacube for one coherent processing interval
$y[l, m]$	Fast time/slow time data matrix for one CPI
$y_s[m]$	Slow-time sequence for one CPI
z	Detected output
$\tilde{z}$	Transformed detected output
Z	Meteorological reflectivity; altitude

Selected Acronyms

The following acronyms are used in this text.

1D, 2D, 3D	One-, Two-, Three-Dimensional
ACF	Autocorrelation Function
A/D	Analog-to-Digital
ADC	Analog-to-Digital Converter
AF	Ambiguity Function
AGC	Automatic Gain Control
AL	Altitude Line
AM	Amplitude Modulation
AOA	Angle of Arrival
ASR	Airport Surveillance Radar
ATI	Along-Track Interferometry
BSR	Beam Sharpening Ratio
BT	Time-Bandwidth Product
CA	Clutter Attenuation
CA-CFAR	Cell-Averaging Constant False Alarm Rate
CCD	Coherent Change Detection
CDF	Cumulative Distribution Function
CF	Characteristic Function
CFAR	Constant False Alarm Rate
CMT	Covariance Matrix Taper
CNR	Clutter-to-Noise Ratio
CPI	Coherent Processing Interval
CRLB	Cramèr-Rao Lower Bound
CRP	Central Reference Point
CRT	Chinese Remainder Theorem
CSI	Clutter Suppression Interferometry
CUT	Cell under Test
CW	Continuous Wave
dB	Decibel
DBS	Doppler Beam Sharpening
dBsm	Decibels relative to 1 square meter
DFT	Discrete Fourier Transform
DOF	Degrees of Freedom
DPCA	Displaced Phase Center Antenna
DSP	Digital Signal Processing
DTED	Digital Terrain Elevation Data

DTFT	Discrete-Time Fourier Transform
EA	Electronic Attack
ECM	Electronic Countermeasures
EKF	Extended Kalman Filter
EM	Electromagnetic
EMI	Electromagnetic Interference
ENOB	Effective Number of Bits
EW	Electronic Warfare
FFT	Fast Fourier Transform
FIR	Finite Impulse Response
FM	Frequency Modulation
FMCW	Frequency-Modulated Continuous Wave
FSK	Frequency Shift Keying
FT	Fourier Transform
GMTI	Ground Moving Target Indication
GOCA CFAR	Greatest-of Cell-Averaging Constant False Alarm Rate
GPS	Global Positioning System
HF	High Frequency
HPRF	High Pulse Repetition Frequency
I	In-Phase
ICM	Internal Clutter Motion; Intrinsic Clutter Motion
IDFT	Inverse Discrete Fourier Transform
IF	Intermediate Frequency
IFFT	Inverse Fast Fourier Transform
IFSAR	Interferometric Synthetic Aperture Radar
i.i.d.	Independent Identically Distributed
IIR	Infinite Impulse Response
IMU	Inertial Measurement Unit
INS	Inertial Navigation System
InSAR	Interferometric Synthetic Aperture Radar
IPD	Interferometric Phase Difference
IPP	Interpulse Period
ISL	Integrated Sidelobe Level; Interference Subspace Leakage
JNR	Jammer-to-Noise Ratio
JSR	Jammer-to-Signal Ratio
KF	Kalman Filter
KT	Keystone Transform/Transformation
LCM	Least Common Multiple
LEO	Low Earth Orbit
LFM	Linear Frequency Modulation
LNA	Low Noise Amplifier
LO	Local Oscillator
LOS	Line of Sight
LPF	Lowpass Filter
LPG	Loss in Processing Gain
LPRF	Low Pulse Repetition Frequency
LRT	Likelihood Ratio Test
LSI	Linear Shift Invariant
MDD	Minimum Detectable Doppler
MDV	Minimum Detectable Velocity

MIMO	Multiple Input, Multiple Output
MLC	Mainlobe Clutter
MLE	Minimum Likelihood Estimate/Estimator/Estimation
MMSE	Minimum Mean-Squared Error/Estimate
MMW	Millimeter Wave
MPRF	Medium Pulse Repetition Frequency
MTD	Moving Target Detector
MTI	Moving Target Indication
MVU	Minimum Variance Unbiased
NEXRAD	Next Generation Radar
NLFM	Nonlinear Frequency Modulation
OS CFAR	Order Statistic Constant False Alarm Rate
PAF	Periodic Ambiguity Function
PD	Pulse Doppler
PDF	Probability Density Function
PF, PFA	Polar Format, Polar Format Algorithm
PGA	Phase Gradient Algorithm
PL	Processing Loss
PM	Phase Modulation
PPP	Pulse Pair Processing
PPS	Pulses per Second
PRF	Pulse Repetition Frequency
PRI	Pulse Repetition Interval
PSD	Power Spectrum/Spectral Density
PSL	Peak Sidelobe Level
PSP	Principle of Stationary Phase
PSR	Point Spread Response
Q	Quadrature
RCS	Radar Cross Section
RD	Range-Doppler
RF	Radar Frequency, Radio Frequency
RFA	Rectangular Format Algorithm
RFI	Radio Frequency Interference
RI	Repetition Interval
RM, RMA	Range Migration, Range Migration Algorithm
RMB	Reed-Mallet-Brennan
RMS	Root Mean Square
ROC	Receiver Operating Characteristic
ROI	Region of Interest
ROS	Region of Support
RP	Range Profile
RR	Repetition Rate
RRE	Radar Range Equation
RV	Random Variable
RVP	Residual Video Phase
SAR	Synthetic Aperture Radar
SB	Sampling Bound
SCR	Signal-to-Clutter Ratio
SIR	Signal-to-Interference Ratio; Shuttle Imaging Radar
SMI	Sample Matrix Inverse

SLC	Sidelobe Clutter
SMTI	Surface Moving Target Indication
SNR	Signal-to-Noise Ratio
SOCA CFAR	Smallest-of Cell-Averaging Constant False Alarm Rate
SQNR	Signal-to-Quantization Noise Ratio
STAP	Space-Time Adaptive Processing
STC	Sensitivity Time Control
T/R	Transmit/Receive
UDSF	Usable Doppler Space Fraction
UHF	Ultra-High Frequency
ULA	Uniform Linear Array
UWB	Ultra Wideband
VA	Virtual Array
VE	Virtual Element
VHF	Very High Frequency
WGN	White Gaussian Noise
ZZB	Ziv-Zakai Bound

Fundamentals of Radar Signal Processing

CHAPTER 1
Introduction to Radar Systems and Signal Processing

1.1 History and Applications of Radar

The word "radar" was originally an acronym, RADAR, for "*ra*dio *d*etection *a*nd *r*anging." Today, the technology is so common that the word has become a standard English noun. Many people have direct personal experience with radar in such applications as measuring fastball speeds or, often to their regret, traffic control.

The history of radar extends to the early days of modern electromagnetic theory (Swords, 1986; Skolnik, 2001). In 1886, Hertz demonstrated reflection of radio waves, and in 1900 Tesla described a concept for electromagnetic detection and velocity measurement in an interview. In 1903 and 1904, the German engineer Hülsmeyer experimented with ship detection by radio wave reflection, an idea advocated again by Marconi in 1922. In that same year, Taylor and Young of the U.S. Naval Research Laboratory (NRL) demonstrated ship detection by radar and in 1930 Hyland, also of NRL, first detected aircraft by radar (albeit accidentally), setting off a more substantial investigation that led to a U.S. patent for what would now be called a *continuous wave* (CW) radar in 1934.

The development of radar accelerated and spread in the middle and late 1930s with largely independent developments in the United States, Britain, France, Germany, Italy, Japan, and Russia. In the United States, R. M. Page of NRL began an effort to develop pulsed radar in 1934, with the first successful demonstrations in 1936. The year 1936 also saw the U.S. Army Signal Corps begin active radar work, leading in 1938 to its first operational system, the SCR-268 antiaircraft fire control system, and in 1939 to the SCR-270 early warning system, the detections of which were tragically ignored at Pearl Harbor. British development, spurred by the threat of war, began in earnest with work by Watson-Watt in 1935. The British demonstrated pulsed radar that year and by 1938 established the famous Chain Home surveillance radar network that remained active until the end of World War II. They also built the first airborne interceptor radar in 1939. In 1940, the United States and Britain began to exchange information on radar development. Up to this time, most radar work was conducted at *high frequency* (HF) and *very high frequency* (VHF) wavelengths; but with the British disclosure of the critical cavity magnetron microwave power tube and the United States' formation of the Radiation Laboratory at the Massachusetts Institute of Technology, the groundwork was laid for the successful development of radar at the microwave frequencies that have predominated ever since.

Each of the other countries mentioned also carried out CW radar experiments, and each fielded operational radars at some time during World War II. Efforts in France and Russia were interrupted by German occupation. On the other hand, Japanese efforts were aided by the capture of U.S. radars in the Philippines and by the disclosure of German technology. The Germans themselves deployed a variety of ground-based, shipboard, and airborne systems. By the end of the war, the value of radar and the advantages of microwave frequencies and pulsed waveforms were widely recognized.

Early radar development was driven by military necessity, and the military is still a major user and developer of radar technology. Military applications include surveillance, navigation, and weapons guidance for ground, sea, air, and space vehicles. Military radars span the range from huge ballistic missile defense systems to fist-sized tactical missile seekers.

Radar now enjoys an increasing range of applications. One of the most common is the police traffic radar used for enforcing speed limits (and measuring the speed of baseballs and tennis serves). Another is the "color weather radar" familiar to every viewer of local television news or numerous online sources. More sophisticated meteorological radar systems are used for large-scale weather monitoring and prediction and atmospheric research. Another radar application that affects many people is found in the air traffic control systems used to guide commercial aircraft both en route and in the vicinity of airports. Aviation also uses radar as one means for determining altitude and avoiding severe weather, and may soon use it to assist in imaging runway approaches in poor weather. Radar is commonly used by the shipping, heavy equipment, and automotive industries for collision avoidance, obstacle detection, and related safety functions. Indeed, one of the most important current drivers in radar technology is the automotive industry, which now places millions of small radars on the road each year in driver assistance systems. Radar is also an essential sensor for emerging autonomous driving systems. Finally, spaceborne and airborne radar is an important tool in mapping earth topology and environmental characteristics such as water and ice conditions, forestry conditions, land usage, and pollution. While this sketch of radar applications is far from exhaustive, it does indicate the breadth of applications of this remarkable technology.

This text tries to present a thorough, straightforward, and consistent description of the signal processing aspects of radar technology, focusing on fundamental range, Doppler, and angle processing techniques common to most radar systems. Previous editions emphasized pulsed over continuous wave radars. However, recent years have seen extensive proliferation of continuous wave radars in the automotive and other industries. Particularly common are linear frequency-modulated CW (linear FMCW) radars, which use many of the same signal processing and data organization techniques as pulsed systems. Consequently, this edition addresses both pulsed and linear FMCW systems, using the common data acquisition and organization construct of a *datacube* to unify their descriptions.

Similarly, because most radars are *monostatic*, meaning the transmitter and receiver antennas are collocated (and in fact are usually the same antenna), they are emphasized over *bistatic* radars where the antennas are significantly separated, though again many of the results apply to both. Finally, the subject is approached from a digital signal processing (DSP) viewpoint as much as practicable, both because most new radar designs rely heavily on digital processing and because this approach can unify concepts and results often treated separately.

1.2 Basic Radar Functions

Most uses of radar can be classified as *detection*, *tracking*, or *imaging*. Higher-level capabilities are built on top of these basic functions. This text addresses all three and the techniques of signal acquisition and interference reduction necessary to perform them.

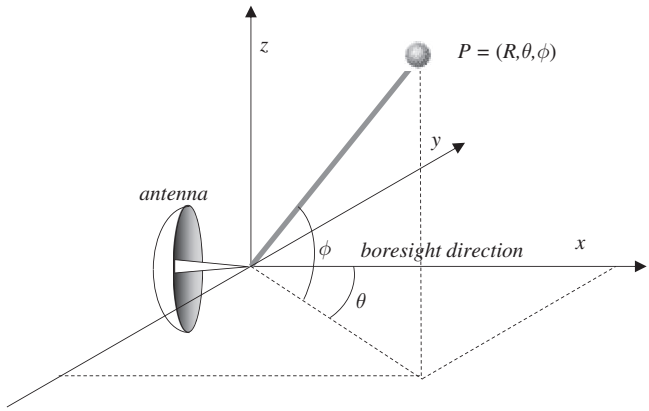

Figure 1.1 Spherical coordinate system for radar measurements.

The most fundamental problem in radar is detection of an object or physical phenomenon. This requires determining whether the receiver output at a given time includes the echo from a reflecting object or only noise or other interference. Detection decisions are usually made by comparing the amplitude $a(t)$ of the receiver output (where t represents time) to a threshold $T(t)$, which may be set a priori in the radar design or may be computed adaptively from the radar data. The time required for a signal to propagate a distance R and return, thus traveling a total distance $2R$, is $2R/c$, where c is the speed of electromagnetic (EM) wave propagation ("speed of light").[1] Therefore, if $a(t) > T(t)$ at some time delay t_0 after a signal is transmitted, it is assumed that a target is present at range

$$R = \frac{ct_0}{2}\text{m} \tag{1.1}$$

Once an object has been detected, it may be desirable to track its location and velocity. A monostatic radar naturally measures position in a spherical coordinate system with its origin at the radar antenna's phase center (defined in Sec. 1.3.4), as shown in Fig. 1.1. In this coordinate system, the antenna look direction, sometimes called the *boresight* direction, is along the $+x$ axis. The angle θ is called the *azimuth* angle, while ϕ is called the *elevation* angle.[2]

The range R to the object is obtained directly from the elapsed time from transmission to detection as just described. Elevation and azimuth angle ϕ and θ are determined from the antenna orientation, since the target must normally be in the antenna field of view to be detected. Velocity is estimated by measuring the Doppler shift of the target echoes. Doppler shift provides only the radial velocity component, but a series of measurements of position and radial velocity can be used to infer target dynamics in all three dimensions.

Because most people are familiar with the idea of following the movement of a "blip" on the radar screen, detection and tracking are the functions most commonly

[1] $c = 2.99792458 \times 10^8$ m/s in a vacuum. A value of $c = 3 \times 10^8$ m/s, normally used except where very high accuracy is required, is used exclusively in this text.

[2] In mathematics, the spherical coordinate system is often defined in terms of range, azimuth angle, and a *polar angle* ϕ_p (also called the *zenith* or *inclination* angle) measured from the z axis. The polar and elevation angles are related as $\phi = \pi/2 - \phi_p$ radians.

associated with radar. However, radars are increasingly used to generate two- and three-dimensional images of an area. Such images can be analyzed for intelligence and surveillance purposes, for topology mapping, or for "earth resources" applications such as analysis of land use, ice cover, deforestation, pollution spills, and so forth. They can also be used for "terrain following" navigation by correlating measured imagery with stored maps. While radar images have not achieved the resolution of optical images, the very low attenuation of electromagnetic waves at microwave frequencies gives radar the important advantage of "seeing" through clouds, fog, and precipitation very well. In addition, radar imagery works day or night because the transmitter provides the "illumination." Consequently, imaging radars generate useful imagery when optical instruments cannot be used at all.

The quality of a radar system is quantified with a variety of figures of merit, depending on the function being considered. In analyzing detection performance, the fundamental parameters are the *probability of detection* P_D and the *probability of false alarm* P_{FA}. If other system parameters are fixed, increasing P_D always requires accepting a higher P_{FA} as well. The achievable combinations are determined by the signal and interference statistics, especially the *signal-to-interference ratio* (SIR). When multiple targets are present in the radar field of view, additional considerations of resolution and sidelobes arise in evaluating detection performance. For example, if two targets cannot be resolved by a radar they will be registered as a single object. If sidelobes are high, the echo from one strongly reflecting target may mask the echo from a nearby but weaker target so that again only one target is registered when two are present. Resolution and sidelobes in range are determined by the radar waveform, while those in angle are determined by the antenna pattern.

In radar tracking, the basic figures of merit are *accuracy* (bias) and *precision* (standard deviation) of the range, angle, and velocity estimates. With appropriate signal processing the achievable accuracy is typically limited by a combination of resolution and SIR. For example, if noise is the primary interference source, the limiting precision often is proportional to $\sqrt{\Delta/SNR}$, where Δ is the resolution in the coordinate of interest and SNR is the value of the *signal-to-noise ratio* (SNR).

In imaging, the principal figures of merit are spatial resolution and dynamic range. Spatial resolution determines what size objects can be distinguished in the final image and therefore to what uses the image can be put. For example, a radar map with 1 km by 1 km resolution would be useful for large-scale land use studies but useless for detailed military surveillance of airfields or missile sites. Dynamic range determines image contrast, which also contributes to the amount of information that can be extracted from an image.

The purpose of signal processing in radar is to extract end products such as detections or images from the raw radar data and to maximize the quality of those products by maximizing resolvability, SIR, and other relevant figures of merit. SIR can be improved by integration of multiple measurements. Resolution and SIR can be jointly improved by matched filters and other waveform design and processing techniques such as frequency agility. Accuracy benefits from increased SIR and interpolation methods. Sidelobe behavior can be improved with the same windowing techniques used in virtually every application of signal processing. Each of these topics is explored in the chapters that follow.

Radar signal processing draws on many of the same techniques and concepts used in other signal processing areas, from such closely related fields as communications and sonar to very different applications such as speech and image processing. Linear filtering and statistical detection theory are central to radar's most fundamental task of target detection. Fourier transforms, implemented using *fast Fourier transform* (FFT) techniques, are ubiquitous, being used for everything from fast convolution implementations of matched filters, to Doppler spectrum estimation, to image formation. Modern model-based spectral estimation and adaptive filtering techniques are used for beamforming and jammer cancellation.

Pattern recognition and, more recently, machine learning techniques are used for target/clutter[3] discrimination and target identification.

At the same time, radar signal processing has several unique qualities that differentiate it from many other signal processing fields. Most modern radars are *coherent*, resulting in a received signal that, once demodulated to baseband, is complex-valued rather than real-valued. Radar signals have very high dynamic ranges of several tens of decibels, in some extreme cases approaching 100 dB. Thus, gain control schemes are common and sidelobe control is often critical to avoid having weak signals masked by stronger ones. In addition, received signals are many decibels weaker than transmitted signals due to propagation and other losses, so that SIR ratios at the receiver are often relatively low. For example, successful detection typically requires an SIR at the point of detection of 10 to 20 dB, but the SIR of the received signal at the antenna will be much less than 0 dB. Large signal processing gains are needed to overcome this deficit.

Another very important distinguishing feature of radar signal processing is the large signal bandwidths compared to most other DSP applications. Instantaneous bandwidths for an individual pulse or CW transmission are frequently on the order of a few megahertz. In some fine resolution[4] radars, they may reach several hundred megahertz and even low gigahertz levels. The difficulty of designing good converters at multi-megahertz or gigahertz sample rates has historically slowed the introduction of digital techniques into radar signal processing for two primary reasons. First, very fast *analog-to-digital* (A/D) converters are required to digitize the high-bandwidth data. Even now that digital techniques are standard in new designs, A/D converter effective word lengths in high-bandwidth systems (high tens of megahertz to ones of gigahertz) are usually a relatively short 8 to 12 bits, rather than the 16 bits common in many other areas.

Second, the high data rates require high-speed computing capability to implement the algorithms. Historically, this meant that it was often necessary to design custom hardware for the digital processor in order to obtain adequate throughput, that is, to "keep up with" the torrent of data. It also meant that radar signal processing algorithms had to be relatively simple compared to lower-bandwidth applications such as sonar in order to minimize the processing load. Only in the late 1990s and later have improved analog semiconductor technology and Moore's law[5] provided enough computing power to host radar algorithms for a wide range of high-performance systems on commercial hardware. This technological progress has enabled rapid development and introduction of new, more complex algorithms to radar signal processing, enabling major improvements in detection, tracking, and imaging capability.

1.3 Elements of a Radar

Figure 1.2 is one possible block diagram of a basic monostatic radar. The waveform generator output is the desired pulse or CW waveform to be transmitted. The transmitter comprises a series of *mixers* and *local oscillators* (LOs) to modulate this waveform to a desired *intermediate*

[3]"Clutter" is an interference signal consisting of unwanted echoes of the radar's transmitted signal from objects not of interest.

[4]Systems exhibiting good or poor resolution are commonly referred to as high- or low-resolution systems, respectively. Since better resolution means a *smaller* numerical value, in this text the terms "fine" and "coarse" are used instead to reduce confusion.

[5]Gordon Moore's famous 1965 prediction was that the number of transistors on an integrated circuit would double every 18 to 24 months. That prediction held remarkably true for at least 40 years, enabling the computing and networking revolutions that began in earnest in the 1980s. Whether it is being maintained, or can be, in the 2020s and later is a perennial subject of debate.

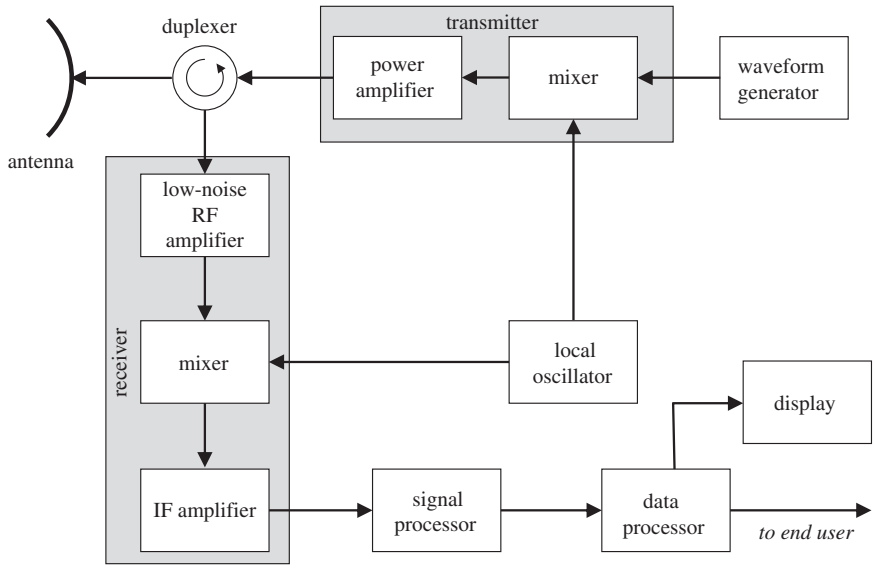

Figure 1.2 Block diagram of a monostatic radar.

frequency (IF) and then to the desired *radio frequency* or *radar frequency* (RF), followed by amplifiers to boost the signal power to a useful level. The transmitter output is routed to the antenna through a *duplexer*, *circulator,* or *T/R switch* (for transmit/receive).

The antenna focuses and concentrates the transmitted radiation into a narrow region of space in a particular direction, providing a power gain to the transmitted signal in that direction. Similarly, it selectively provides greater sensitivity on receive to echoes from that same direction. In doing so, the antenna both amplifies weak target echo signals and localizes them in azimuth and elevation.

The returning echoes are routed by the duplexer into the radar receiver. The receiver is usually a superheterodyne design (Bruder, 2010), and often the first stage is a low-noise RF amplifier. This is followed by one or more stages of demodulation of the received signal to successively lower IFs and ultimately to *baseband*, where the signal is not modulated onto any carrier frequency.

The baseband signal is next sent to the *signal processor*, which performs some or all of a variety of functions such as matched filtering, Doppler filtering, integration, and motion compensation. The output of the signal processor typically becomes the input to a *data processor*. Typical data processor functions might include target classification, target tracking, or image processing operations, depending on the radar purpose. The data processor output is sent to the system display, passed to other systems, or both as appropriate. The distinction between the signal processor and the data processor is somewhat arbitrary. Generally, the signal processor is associated with "lower" level, higher speed, streaming operations, while the data processor is associated with "higher" level operations that tend to be more data-dependent but require less computation.

The configuration of Fig. 1.2 is not unique. For example, many systems perform some of the signal processing functions at IF rather than baseband; matched filtering and some forms of Doppler filtering are common examples. Also, radars differ in which portions of the signal flow are analog and which are digital. Older systems are all analog, and many currently operational systems do not digitize the signal until it is converted to baseband. Thus, any

signal processing performed at IF must be done with analog techniques. Increasingly, new designs digitize the received signal at an IF or even RF stage, moving the A/D converter closer to the radar front end and performing more of the processing digitally. Waveform generation is also done digitally in many modern systems.

The next few subsections provide some additional detail on these major radar subsystems and also discuss some additional radar systems issues.

1.3.1 Radar Frequencies

Radar systems have been operated at frequencies as low as 2 MHz and as high as 220 GHz (Skolnik, 2001); laser radars operate at frequencies on the order of 10^{12} to 10^{15} Hz, corresponding to wavelengths of 0.3 to 30 μm (Jelalian, 1992). However, most radars operate in the microwave frequency region of about 200 MHz to about 30 GHz, with corresponding wavelengths of 0.67 m to 1 cm. There are also numerous systems in the *millimeter wave* (MMW) region of 30 to 300 GHz (1 cm to 1 mm), especially in the 35 and 95 GHz regions. Table 1.1 summarizes the letter nomenclature used for the common nominal radar bands (IEEE, 2019).

Band	Frequencies	Wavelengths	Common Uses
HF	3–30 MHz	100–10 m	Over-the-horizon surveillance
VHF	30–300 MHz	10–1 m	Long range surveillance, foliage penetration, ground penetrating radar, counter-stealth
UHF	300 MHz–1 GHz	1–30 cm	Long range surveillance, foliage penetration
L	1–2 GHz	30–15 cm	Long range surveillance, long range air traffic control
S	2–4 GHz	15–7.5 cm	Moderate range surveillance, terminal air traffic control, airborne early warning, long range weather observation
C	4–8 GHz	7.5–3.75 cm	Long range tracking, weather observation, weapon location
X	8–12 GHz	3.75–2.5 cm	Short range tracking, missile guidance, marine radar, ground imaging, airborne intercept, weapon location
K_u	12–18 GHz	2.5–1.67 cm	High resolution mapping, satellite altimetry, UAV radar
K	18–27 GHz	1.67–1.11 cm	Police radar, automotive radar
K_a	27–40 GHz	1.11 cm–7.5 mm	Short-range fine resolution imaging, airport surveillance
V	40–75 GHz	7.5–4 mm	Scientific remote sensing
W	75–110 GHz	4–2.73 mm	Automotive radar, missile seekers, very fine resolution imaging
Millimeter wave (includes V and W)	30–300 GHz	1 cm–1 mm	Experimental

Table 1.1 Letter Nomenclature and Common Uses for Nominal Radar Frequency Bands

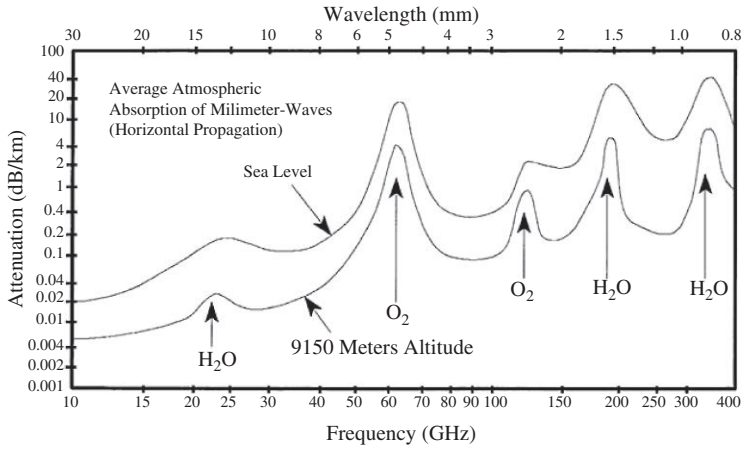

Figure 1.3 One-way atmospheric attenuation of electromagnetic waves. (*Source: EW and Radar Systems Engineering Handbook*, Naval Air Warfare Center, Weapons Division, http://ewhdbks.mugu.navy.mil/.)

Not all frequencies in these bands are suitable for or available to radar operation. Within the HF to K_a bands, specific frequencies are allocated by international agreement to radar operation. At frequencies above X band, atmospheric attenuation of electromagnetic waves becomes significant. Consequently, radars in these bands usually operate at one of several "atmospheric window" frequencies where attenuation is relatively low. Figure 1.3 illustrates the atmospheric attenuation for one-way propagation over the most common radar frequency ranges under approximately "clear air" atmospheric conditions. Most K_a band radars operate near 35 GHz and most W band systems operate near 95 GHz because of the relatively low atmospheric attenuation at these wavelengths.

Lower radar frequencies tend to be preferred for longer range surveillance applications because of the low atmospheric attenuation and high power available in transmitters at these frequencies. Higher frequencies tend to be preferred for finer resolution, shorter range applications due to the smaller achievable antenna beamwidths for a given antenna size, higher attenuation, and lower available transmitter powers.

Weather conditions can also have a significant effect on radar signal propagation. Figure 1.4 illustrates the additional one-way loss as a function of radar frequency for rain rates ranging from a drizzle to a tropical downpour. X-band frequencies (typically about 10 GHz) and below are affected significantly only by very severe rainfall, while MMW frequencies suffer severe losses for even light-to-medium rain rates.

1.3.2 Radar Waveforms and Transmitters

The radar *waveform* is the term for the signal that is modulated onto the RF carrier for transmission, echo reception, and demodulation. It plays a major role in determining the sensitivity and range resolution of the radar. There are many different waveforms in common use. They can all be classified as either pulsed or continuous wave. Figure 1.5 illustrates the difference between the two. The CW waveform of Fig. 1.5*a*, as its name suggests, simply radiates a sinusoidal signal at the desired RF continuously. The pulsed waveform in Fig. 1.5*b* transmits a series of finite length pulses. The series is described by the pulse length τ and either the *pulse repetition interval* (PRI) T between pulses or its inverse, the *pulse repetition frequency* (PRF).

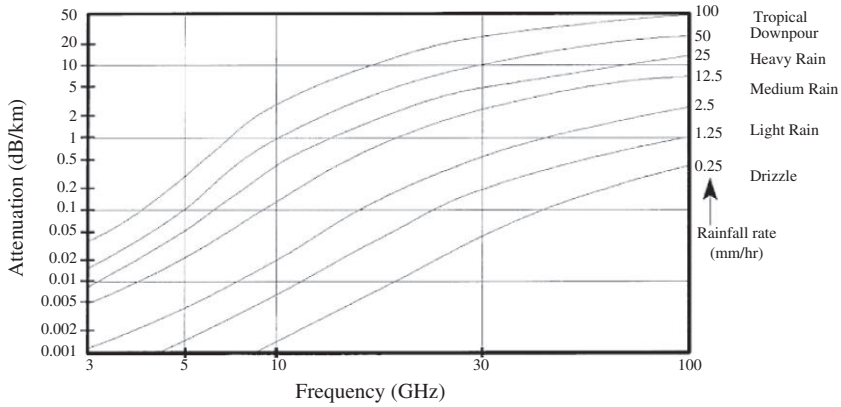

Figure 1.4 Effect of different rates of precipitation on one-way atmospheric attenuation of electromagnetic waves. (*Source: EW and Radar Systems Engineering Handbook*, Naval Air Warfare Center, Weapons Division, http://ewhdbks.mugu.navy.mil/.)

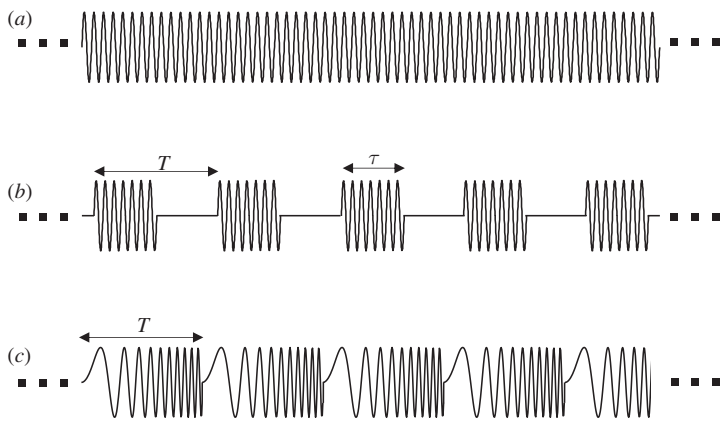

Figure 1.5 Three of the major classes of radar waveforms. (*a*) Continuous wave (CW). (*b*) Pulsed. (*c*) Frequency-modulated continuous wave (FMCW).

The pulsed waveform enables easy measurement of range by observing the time delay between transmission of a pulse and reception of an echo; see Eq. (1.1). Because the CW waveform lacks any distinguishing timing mark such as a pulse edge, another means is needed to measure range. One solution is to modulate the CW waveform with a repeating pattern. Currently the most common example is FMCW. Figure 1.5*c* illustrates an example wherein the frequency of the CW waveform is swept over some bandwidth repeatedly. The duration of one sweep is analogous to the PRI for a pulsed waveform. In the example shown, the sweep rate is constant so that the frequency increases linearly during the sweep interval.

Pulsed waveforms can also exhibit intra-pulse modulation. Both phase- and frequency-modulated pulses are common. Because of their widespread use, in this text the focus will be on pulsed waveforms with phase, frequency, or no modulation, and on linear FMCW waveforms. The details of each are the subject of Chap. 4.

The radar transmitter modulates the waveform to the RF and amplifies it to a useful level. Radar transmitters operate at peak powers ranging from milliwatts to in excess of 10 MW. A wide variety of technologies are used, from solid state sources at lower powers to various vacuum tube devices such as magnetrons and traveling wave tubes at high powers. An excellent survey of transmitter technologies and issues is given in Wallace et al. (2010). High peak power systems are invariably pulsed; CW systems have much lower peak powers. One of the more powerful existing pulsed transmitters is found in the AN/FPS-108 COBRA DANE radar, which has a peak power of 15.4 MW (Brookner, 1988). In pulsed radars the PRF varies widely but is typically between several hundred and several tens of thousands of pulses per second (PPS); in some modern integrated "radar-on-a-chip" systems, the PRF can be several hundred thousand PPS. The duty cycle of pulsed systems is usually relatively low and often well below 1 percent, so that average powers rarely exceed 10 to 20 kW. COBRA DANE again offers an extreme example with its high average power of 0.92 MW. Pulse lengths are most often between about 100 ns and 100 μs, though some systems use pulses as short as a few nanoseconds while others have extremely long pulses, on the order of 1 ms or more.

It will be seen in Chap. 6 that the detection performance achievable by a radar improves with the amount of energy in the transmitted waveform. Maximizing energy suggests that a radar waveform should be as long as feasible and be transmitted at maximum power. To satisfy the second condition, radars generally do not use amplitude modulation of the transmitted waveform since that implies that at least a part of the waveform is transmitted at less than full power.

Waveform length is a more complicated issue. It will be seen in Chap. 4 that the nominal range resolution ΔR is determined by the waveform bandwidth β in hertz:

$$\Delta R = \frac{c}{2\beta}\,\mathrm{m} \tag{1.2}$$

For an unmodulated pulse, the bandwidth is inversely proportional to its duration. Fine resolution therefore implies shorter pulses, in conflict with the need for longer pulses to maximize energy. To increase waveform bandwidth for a given pulse length without sacrificing energy, many radars routinely use phase or frequency modulation of the pulse. Similar issues apply to FMCW waveforms. Desirable values of range resolution vary from a few kilometers in long-range surveillance systems, which tend to operate at lower RFs, to a meter or less in very fine-resolution imaging systems, which tend to operate at high RFs. Corresponding waveform bandwidths are on the order of 100 kHz to 1 GHz. These bandwidths are typically 1 percent or less of the RF. Few radars achieve 10 percent bandwidth, though some achieve bandwidths of 25 percent of the RF or greater, qualifying them as *ultrawideband* (UWB) radars (IEEE, 2017). Nonetheless, most radar waveforms can be considered narrowband, bandpass functions.

1.3.3 Antennas

The antenna plays a major role in determining the sensitivity and angular resolution of the radar. A very wide variety of antenna types are used in radar systems. Some of the more common types are parabolic reflector antennas, scanning feed antennas, lens antennas, and phased array antennas.

From a signal processing perspective, the most important properties of an antenna are its gain, beamwidth, and sidelobe levels. Each of these follows from consideration of the antenna *power pattern*. The one-way power pattern $P(\theta, \phi)$ describes the radiation intensity during transmission in the direction (θ, ϕ) relative to the antenna boresight. Aside from scale factors, which are unimportant for normalized patterns, it is related to

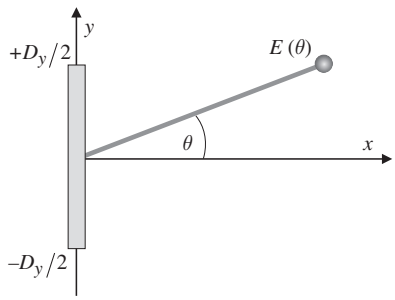

Figure 1.6 Geometry for one-dimensional electric field calculation on a linear aperture.

the radiated electric field intensity $E(\theta, \phi)$, known as the antenna one-way *voltage pattern*, according to

$$P(\theta, \phi) = |E(\theta, \phi)|^2 \tag{1.3}$$

For a rectangular aperture with an illumination function that is separable in the two aperture dimensions, $P(\theta, \phi)$ can be factored as the product of separate one-dimensional patterns (Stutzman and Thiele, 2012):

$$P(\theta, \phi) = P_\theta(\theta)\, P_\phi(\phi) \tag{1.4}$$

For most radar scenarios, only the *far field* (also called *Fraunhofer*) power pattern is of interest. The far-field is conventionally defined to begin at a range of D^2/λ_t or $2D^2/\lambda_t$ for an antenna of aperture size D. Consider the azimuth (θ) pattern of the one-dimensional linear aperture geometry shown in Fig. 1.6. From a signal processing viewpoint, an important property of aperture antennas such as flat plate arrays and parabolic reflectors is that the electric field intensity as a function of azimuth $E(\theta)$ in the far field is the inverse Fourier transform[6] of the distribution $A(y)$ of current across the aperture in the azimuth plane (Bracewell, 1999; Skolnik, 2001),

$$E(\theta) = \int_{-D_y/2}^{D_y/2} A(y) \exp[j(2\pi y/\lambda_t)\sin\theta]\, dy \tag{1.5}$$

where the "frequency" variable is the *spatial frequency* or *wavenumber* $(2\pi/\lambda_t)\sin\theta$ and is in units of radians per meter. The idea of spatial frequency is discussed in App. B.

To be more explicit about this point, define $s = \sin\theta$ and $\zeta = y/\lambda_t$. Substituting these definitions in Eq. (1.5) gives

$$\frac{1}{\lambda_t} \int_{-D_y/2\lambda_t}^{D_y/2\lambda_t} A(\lambda_t \zeta) \exp(j2\pi\zeta s)\, d\zeta = E(s) \tag{1.6}$$

which is clearly of the form of an inverse Fourier transform. (The finite integral limits are due to the finite support of the aperture.) Because of the definitions of ζ and s, this transform

[6]Whether it is the forward or inverse Fourier transform (FT) depends on the FT definition one uses. This text uses the electrical engineering convention, in which the sign of the argument of the exponential in the FT kernel is negative for the forward transform and positive for the inverse.

relates the current distribution as a function of aperture position normalized by the wavelength to a spatial frequency variable that is related to the azimuth angle through a nonlinear mapping. It of course follows that

$$A(\lambda_t \zeta) = \int_{-\infty}^{+\infty} E(s) \exp(-j2\pi\zeta s)\, ds \tag{1.7}$$

The infinite limits in Eq. (1.7) are misleading, since the variable of integration $s = \sin\theta$ can only range from -1 to $+1$. Because of this, $E(s)$ is taken to be zero outside of this range on s.

Equation (1.7) is a somewhat simplified expression that neglects a range-dependent overall phase factor and a slight amplitude dependence on range (Balanis, 2016). This Fourier transform property of antenna patterns will allow the use of linear system concepts in Chap. 2 to understand the effects of the antenna on cross-range resolution and the angular sampling densities needed to avoid spatial aliasing.

An important special case of Eq. (1.5) occurs when the aperture current illumination is a constant, $A(y) = A_0$. The far-field one-way voltage pattern, normalized to its peak, is then the familiar sinc function

$$E(\theta) = \frac{\sin[\pi(D_y/\lambda_t)\sin\theta]}{\pi(D_y/\lambda_t)\sin\theta} \tag{1.8}$$

The magnitude of $E(\theta)$ is illustrated in Fig. 1.7 for the case $D_y = 6\lambda_t$, along with the definitions for three important figures of merit of an antenna pattern. The pattern exhibits the typical structure of a high-gain mainlobe surrounded by low-gain sidelobes. The angular resolution of the antenna is determined primarily by the width of its mainlobe. The mainlobe width is conventionally quantified by the *3-dB beamwidth*, which is the width of the mainlobe

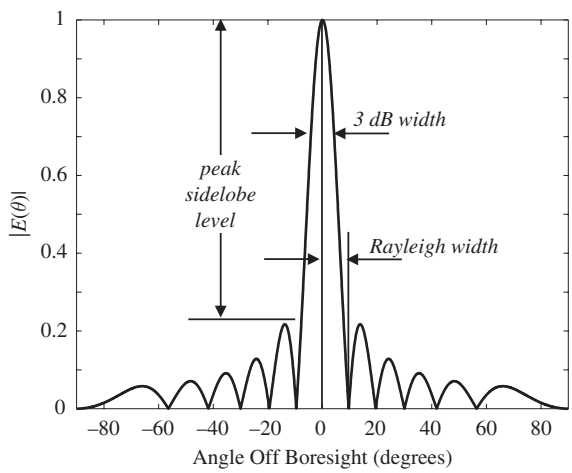

Figure 1.7 One-way radiation pattern of a uniformly illuminated aperture with $D_y = 6\lambda_t$. The 3-dB beamwidth, Rayleigh beamwidth, and peak sidelobe definitions are illustrated.

between the points where $|E(\theta)|^2$ is reduced by 3 dB (approximately one-half) from its peak at $\theta = 0$. This can be determined by setting $E(\theta) = 1/\sqrt{2} \approx 0.707$ and solving for the argument $\alpha = \pi (D_y/\lambda_t)\sin\theta$. The answer is found numerically to be $\alpha = 1.4$, which occurs at the angle $\theta_0 = \sin^{-1}(1.4\lambda_t/\pi D_y)$. The 3-dB beamwidth extends from $-\theta_0$ to $+\theta_0$ and is therefore

$$\text{3-dB beamwidth} = \theta_3 = 2\sin^{-1}\left(\frac{1.4\lambda_t}{\pi D_y}\right) \approx 0.89\frac{\lambda_t}{D_y} \text{ radians} \tag{1.9}$$

The small-angle approximation used in the last step holds for most radar antenna beamwidths.

Although 3-dB beamwidths are traditional, for analysis the Rayleigh beamwidth is often simpler to compute. This is the one-sided width of the mainlobe from its peak to its first null, and is given by (see Prob. 7)

$$\theta_R = \sin^{-1}\left(\frac{\lambda_t}{D_y}\right) \approx \frac{\lambda_t}{D_y} \text{ radians} \tag{1.10}$$

For the constant aperture illumination case, the Rayleigh beamwidth also happens to equal the 4-dB beamwidth. This is not true for antennas in general. Finally, the null-to-null beamwidth θ_{nn} is simply twice the Rayleigh beamwidth, encompassing the entire mainlobe.

Whichever metric is used, note that a smaller beamwidth requires a larger aperture or a shorter wavelength. Typical beamwidths range from as little as a few tenths of a degree to several degrees for a *pencil beam antenna*, where the beam is made as narrow as possible in both azimuth and elevation. Some antennas are deliberately designed to have broad vertical beamwidths of several tens of degrees for convenience in large volume search; these designs are called *fan beam antennas*.

The *peak sidelobe* of the pattern affects how echoes from one object affect the detection of neighboring objects. For the uniform illumination pattern, the peak sidelobe is 13.2 dB below the mainlobe peak. This is often considered insufficient in radar systems because strong unwanted signals entering the antenna from the sidelobe directions may not be attenuated enough to enable detection of weaker target echoes in the mainlobe direction. Antenna sidelobes can be reduced by use of a nonuniform aperture distribution (Skolnik, 2001), sometimes referred to as *tapering, shading, or apodization of* the antenna. In fact, this is no different from the window or weighting functions used for sidelobe control in other areas of signal processing such as spectrum analysis and digital filter design, and peak sidelobes can easily be reduced to around 25 to 40 dB at the expense of an increase in mainlobe width (see App. B). Lower sidelobes are possible but may be increasingly difficult to achieve due to manufacturing imperfections and inherent design limitations.

The antenna *power gain G* is the ratio of peak radiation intensity from the antenna to the radiation that would be observed from a lossless, isotropic (omnidirectional) antenna if both have the same input power. Power gain is determined by both the antenna pattern and by losses in the antenna. A useful rule of thumb for a typical antenna is (Stutzman, 1998)

$$\begin{aligned} G &\approx \frac{26{,}000}{\theta_3\phi_3} \quad (\theta_3, \phi_3 \text{ in degrees}) \\ &\approx \frac{7.9}{\theta_3\phi_3} \quad (\theta_3, \phi_3 \text{ in radians}) \end{aligned} \tag{1.11}$$

Though both higher and lower values are possible, typical radar antennas have gains from about 10 dB for a broad fan-beam search antenna to approximately 40 dB for a pencil beam that might be used for both search and track.

Effective aperture A_e is an important characteristic in describing the behavior of an antenna being used for reception. Suppose a wave with power density W W/m^2 incident on the antenna results in a power P delivered to the antenna load. The effective aperture is defined as the ratio (Balanis, 2016)

$$A_e = \frac{P}{W} \text{ m}^2 \tag{1.12}$$

Note that A_e is not the actual physical area of the antenna. It is the fictional area such that, if all of the power incident on that area was collected and delivered to the load with no loss, it would account for all of the observed power output of the actual antenna. Effective aperture is directly related to antenna *directivity*, which in turn is related to antenna gain and efficiency. For most antennas, the efficiency is near unity and the effective aperture and gain are related by (Balanis, 2016)

$$G = \frac{4\pi}{\lambda_t^2} A_e \tag{1.13}$$

Another important type of antenna is the *array antenna*. An array antenna is one composed of a collection of individual antennas called array *elements*. The elements are typically identical dipoles or other simple antennas with very broad patterns. Usually, the elements are evenly spaced to form a *uniform linear array* (ULA) as shown in one dimension in Fig. 1.8. Figure 1.9 illustrates examples of real array and aperture antennas. Many more examples are given in Chaps. 1 and 9 in Richards et al. (2010).

The voltage pattern for the linear array is most easily arrived at by considering the antenna in its receive mode. Suppose the rightmost element is taken as a reference point, there are N elements in the array, and the elements are isotropic (constant gain for all θ). The signal in branch n is weighted with the complex weight a_n. The incoming electric field voltage $E_0 \exp(j\Omega_t t)$ at the reference element will also appear at each of the other elements, but delayed in time by an additional $d \sin\theta / c$ from each element to the next due to the increasing propagation distance to each. The total output voltage will be the sum of the time-shifted and weighted outputs of all of the array elements. The amplitude of the output voltage is (Skolnik, 2001; Stutzman and Thiele, 2012; or see Sec. 9.2)

$$E(\theta) = E_0 \sum_{n=0}^{N-1} a_n \exp[j(2\pi/\lambda_t) n d \sin\theta] \tag{1.14}$$

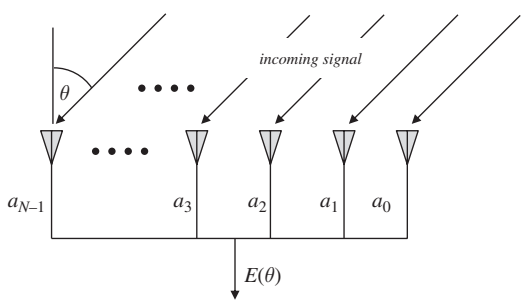

Figure 1.8 Geometry of the uniform linear array antenna.

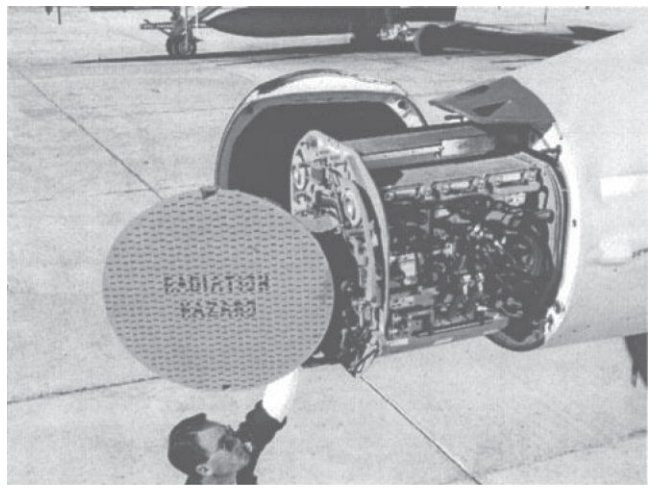

(*a*)

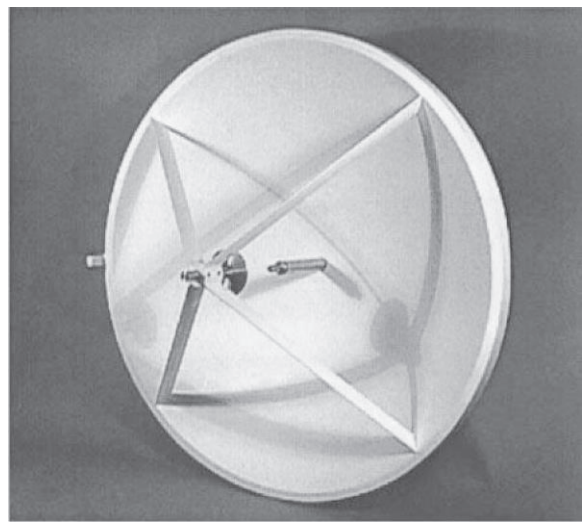

(*b*)

Figure 1.9 Examples of typical array and aperture antennas. (*a*) Slotted phased array in the nose of an F/A-18 aircraft. This antenna is part of the AN/APG-73 radar system. (*b*) A Cassegrain reflector antenna. [Image (*a*) courtesy of Raytheon Technologies. Image (*b*) courtesy of Quinstar Corp. Used with permission.]

This is similar in form to the inverse *discrete Fourier transform* (DFT) of the weight sequence $\{a_n\}$. Like the aperture antenna, the antenna pattern of the linear array thus involves a Fourier transform, this time of the weight sequence. For the case where all the $a_n = 1$, the pattern is the familiar "aliased sinc" (asinc) function,[7] whose magnitude is

[7]Also called the digital sinc (dsinc) or Dirichlet function. It is the discrete-variable equivalent of the usual continuous-variable sinc function.

$$|E(\theta)| = E_0 \left| \frac{\sin[N(\pi d/\lambda_t)\sin\theta]}{\sin[(\pi d/\lambda_t)\sin\theta]} \right| \tag{1.15}$$

This function is very similar to that of Eq. (1.8) and Fig. 1.7. If the number of elements N is reasonably large (nine or more) and the product Nd is considered to be the total aperture size D, the 3-dB beamwidth is $0.89\lambda_t/D$, and the first sidelobe is 13.2 dB below the mainlobe peak; both numbers are the same as those of the uniformly illuminated aperture antenna. By varying the amplitudes of the weights a_n, it is possible to reduce the sidelobes at the expense of a broader mainlobe and a reduction in output SNR.

Actual array elements are not isotropic radiators. A simple model often used as a first-order approximation to a typical element pattern $E_{el}(\theta)$ is

$$E_{el}(\theta) \approx \cos\theta \tag{1.16}$$

The right-hand side of Eq. (1.15) is then called the *array factor* $AF(\theta)$, and the composite radiation pattern becomes

$$E(\theta) = AF(\theta)E_{el}(\theta) \tag{1.17}$$

Because the cosine function is slowly varying in θ, the beamwidth and first sidelobe level are not greatly changed by including the element pattern for signals arriving at angles near broadside (near $\theta = 0$). The element pattern does reduce distant sidelobes, thereby reducing sensitivity to waves impinging on the array from well off broadside.

The discussion so far has been phrased in terms of the transmit antenna pattern (for aperture antennas) or the receive pattern (for arrays), but not both. The patterns described have been *one-way antenna patterns*. The reciprocity theorem guarantees that the receive antenna pattern is identical to the transmit antenna pattern (Balanis, 2016). Consequently, for a monostatic radar, the *two-way antenna pattern* (power or voltage) is just the square of the corresponding one-way pattern. It also follows that the antenna phase center location is the same in both transmit and receive modes.

1.3.4 Virtual Elements and Virtual Arrays

Two more useful antenna concepts are the antenna *phase front* (or *wave front*) and *phase center* (Sherman, 2011; IEEE, 2014; Balanis, 2016; Richards, 2018). A phase front of a radiating antenna is any surface on which the phase of the field is a constant. In the far-field, the phase fronts are usually approximately spherical, at least over localized regions. The phase center of the antenna is the center of curvature of the phase fronts. Put another way, the phase center is the point at which an isotropic radiator should be located so that the resulting phase fronts best match those of the actual antenna. The phase center concept is useful because it defines an effective location of the antenna, which can in turn be used for analyzing effective path lengths, Doppler shifts, and so forth. For symmetrically illuminated aperture antennas, the phase center will be centered in the aperture plane but may be displaced forward or backward from the actual aperture. Referring to Fig. 1.6, the phase center would occur at $y = 0$ but possibly $x \neq 0$, depending on the detailed antenna shape.

The phase center idea is especially useful in developing the *virtual array* (VA) concept for analyzing situations where the transmit and receive antennas are not collocated due either to actual physical separation or to platform motion between transmission and reception times. Consider the situation in Fig. 1.10, which shows separate transmit and receive antenna elements at coordinates x_T and x_R and a point scatterer **P** in the far-field. It is straightforward to show that the phase shift of the signal transmitted from x_T and received at x_R (total path length equal to $R_R + R_T$) is, to a good approximation, the same as that of a signal transmitted from and received at the *virtual element* (VE) location **VE** halfway between the two (total path

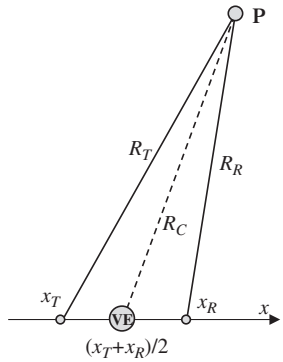

Figure 1.10 Virtual element corresponding to a transmit and receive element pair.

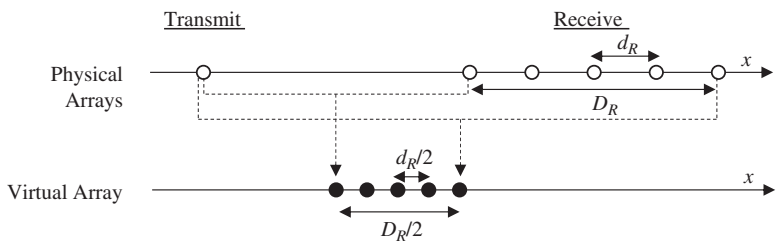

Figure 1.11 Virtual array formed by paring one transmit element with five independent receive elements. (The virtual array has been offset vertically for clarity.)

length $2R_C$) (Richards, 2018). Consequently, for analysis purposes the transmit and receive elements can be replaced by the single VE. This substitution will be useful in the discussion of ground moving target indication in Chap. 5.

Now consider the configuration of Fig. 1.11. The transmit antenna is the single isotropic white element on the left. The receive antenna is the five-element uniform linear array of white elements with element spacing d_R and total aperture size D_R on the right. The signal received by the leftmost element of the receive array will be essentially identical to one transmitted and received by a VE located halfway between it and the transmit element. This location is the leftmost of the five black elements forming the VA, as shown by the dotted line. (The VA will actually be located on the same x-axis line as the transmit and receive elements; it is offset vertically in the figure for clarity.) Each of the five transmit-receive element pairings generates a VE. These collectively form the five-element VA shown. Note that the element spacing and overall aperture size are half the physical receive array spacing and size.

The VE and VA concepts can be used to provide a common analysis framework for a variety of problems in antenna design, synthetic aperture analysis (Chap. 8), and emerging techniques such as multi-input, multi-output (MIMO) radar. Much more detail on these concepts is available in Richards (2018) and Richards (2019).

1.3.5 Receivers

It was shown in Sec. 1.3.2 that radar signals are usually narrowband, bandpass (because they are on a carrier frequency), phase- or frequency-modulated functions.

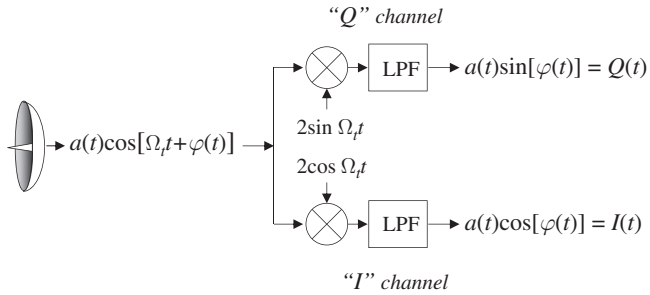

Figure 1.12 Quadrature or "I/Q" channel receiver model.

This means that the echo waveform $\overline{y}(t)$ received from a single scatterer can be modeled in the form

$$\overline{y}(t) = a(t)\cos[\Omega_t t + \varphi(t)] \tag{1.18}$$

Here Ω_t is the nominal RF in radians per second; $\varphi(t)$ is the phase modulation (PM) function, which also includes frequency modulation as a special case; and $a(t)$ is the amplitude modulation (AM). In a CW system, $a(t)$ would be a constant. In the simplest pulsed systems, $a(t)$ would be just a rectangular pulse envelope. In a constant frequency pulsed or CW system (no FM or PM), $\varphi(t)$ would be a constant. The major function of the receiver processing is demodulation of the information-bearing part of the radar signal to baseband with the goal of estimating $a(t)$ and $\varphi(t)$.

Figure 1.12 illustrates the signal processor's simplified view of the receiver structure used in most classical radars. The lower channel mixes the received signal with a local oscillator at the radar frequency. The output of the mixer is the product of its two input signals. Applying a trigonometric identity, the mixer is seen to generate both sum and difference frequency components at its output:

$$2\cos(\Omega_t t) \cdot a(t)\cos[\Omega_t t + \varphi(t)] = a(t)\cos(\Omega_t t) + a(t)\cos[2\Omega_t t + \varphi(t)] \tag{1.19}$$

The high-frequency sum frequency term is then removed by the lowpass filter (LPF), leaving only the difference frequency, also called the *beat frequency*. Note that the difference frequency is taken to be the received echo frequency minus the reference oscillator frequency. In this case, the beat frequency is zero so the output is just the modulation term $a(t)\cos[\varphi(t)]$. The upper channel mixes the signal with a *quadrature* oscillator having the same frequency but a 90° phase shift as compared to the lower channel oscillator. The upper channel mixer output is

$$2\sin(\Omega_t t) \cdot a(t)\cos[\Omega_t t + \varphi(t)] = a(t)\sin(\Omega_t t) + a(t)\sin[2\Omega_t t + \varphi(t)] \tag{1.20}$$

which, after filtering, leaves the modulation term $a(t)\sin[\varphi(t)]$.

If the input $\overline{x}(t)$ is written as $a(t)\sin[\Omega_t t + \varphi(t)]$ instead, the lower and upper channel outputs are interchanged. Whichever form is used for the input, the receiver channel having an output proportional to the cosine of the input phase is called the *in-phase* or "I" channel; the other is called the *quadrature* phase or "Q" channel.

Both the I and Q channels are needed to unambiguously determine the amplitude and phase of the echo. Suppose only the I channel is implemented in the receiver, giving the single measured value $a(t)\cos[\varphi(t)]$. There are an infinite number of combinations of a and

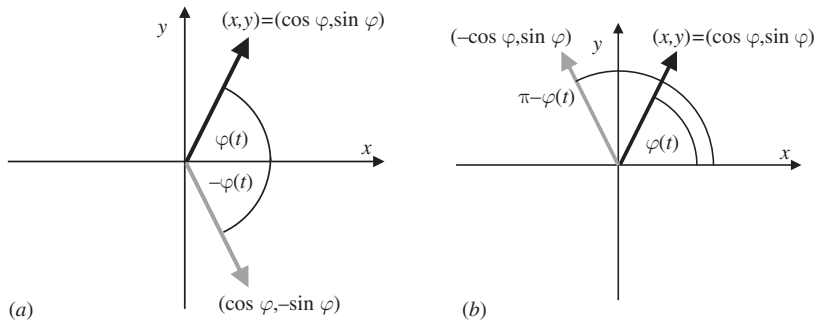

Figure 1.13 (*a*) The I channel of the receiver in Fig. 1.12 measures only the cosine of the phasor $\theta(t)$. (*b*) The Q channel measures only the sine of the phasor.

φ that produce the same product; the I measurement alone is not sufficient to specify both. However, if the Q channel measurement $a(t)\sin[\varphi(t)]$ is also available, the amplitude can be found as $a(t) = \sqrt{I^2(t) + Q^2(t)}$.

Knowing $a(t)$ is still not sufficient to determine $\varphi(t)$ using only one of the I or Q measurements. Figure 1.13 illustrates the problem. In Fig. 1.13*a* the signal phase $\varphi(t)$ is represented as a unit-magnitude black phasor in the complex plane; the amplitude $a(t)$ has been removed. If only the I channel is implemented in the receiver, only the cosine of $\varphi(t)$ will be measured. In this case, the true phasor will be indistinguishable from the gray phasor $-\varphi(t)$. Similarly, if only the Q channel is implemented so that only the sine of $\varphi(t)$ is measured, then the true phasor will be indistinguishable from the gray phasor of Fig. 1.13*b*, which corresponds to $\pi - \varphi(t)$. When both the I and Q channels are implemented, the phasor quadrant is determined unambiguously.[8]

In modern coherent radars, the signal processor will normally assign the I signal to be the real part and the Q signal to be the imaginary part of a new complex signal

$$x(t) = I(t) + jQ(t) = a(t)\exp[j\varphi(t)] \tag{1.21}$$

Equation (1.21) implies a more convenient way of representing the effect of an ideal coherent receiver on a transmitted signal. Instead of representing the transmitted signal by a cosine function, an equivalent complex exponential function is used instead.[9] The received echo signal of Eq. (1.18) is thus replaced by

$$\overline{x}(t) = a(t)\exp[\Omega_t t + \varphi(t)] \tag{1.22}$$

The receiver structure of Fig. 1.12 can then be replaced with the simplified model of Fig. 1.14, where the echo is demodulated by multiplication with a complex reference oscillator $\exp(-j\Omega_t t)$.

[8]This is analogous to the use of the two-argument `atan2()` function instead of the single-argument `atan()` function in many programming languages.

[9]Although these formalizations are not needed for the discussions in this text and are therefore avoided for simplicity, it is worthwhile to note that the complex signal in Eq. (1.22) is the *analytic signal* associated with the real-valued signal of Eq. (1.18). The imaginary part of Eq. (1.22) is the *Hilbert transform* of the real part (Papoulis, 1987; Bracewell, 1999).

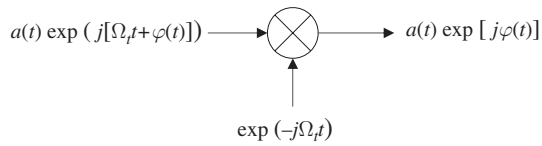

Figure 1.14 Simplified transmission and receiver model using complex exponential signals.

This technique of modeling the transmitted and received real-valued signals by equivalent complex signals using a corresponding complex demodulator produces exactly the same output result obtained in Eq. (1.21) by explicitly modeling the real-valued signals and the I and Q channels, but is much more compact and easier to manipulate. This complex exponential analysis approach is used throughout the remainder of the book. It is important to remember that this is an analysis technique; actual analog hardware must still operate with real-valued signals only. However, once signals are digitized, they may be treated explicitly as complex signals in the digital processor.

Figure 1.12 implies several requirements on a high-quality receiver design. For example, the local oscillator frequencies in the transmitter modulator and receiver demodulator must be identical. This is usually ensured by having a single *stable local oscillator* (STALO) in the radar system that provides a frequency reference for both. Furthermore, many types of radar processing require *coherent* operation. The IEEE *Standard Radar Definitions* defines "coherent signal processing" as "echo integration, filtering, or detection using amplitude *and phase* of the signal referred to a coherent oscillator" (emphasis added) (IEEE, 2017). Coherency is a stronger requirement than frequency stability. In practice, it means that the transmitted carrier signal must have a fixed phase reference for several, perhaps many, consecutive pulses or CW sweeps. Consider a pulse transmitted at time zero of the form $a(t)\cos(\Omega_t t + \varphi)$, where $a(t)$ is the pulse shape. In a coherent system, a pulse transmitted T seconds later will be of the form $a(t - T)\cos(\Omega_t t + \varphi)$. Note that both pulses have the same argument for their cosine term. Only the envelope term is delayed, shifting the pulse location on the time axis while keeping the same underlying sinusoid. An example of a noncoherently related second pulse would be $a(t - T)\cos[\Omega_t(t - T) + \varphi] = a(t - T)\cos[\Omega_t t + (\varphi - \Omega_t T)]$, which is nonzero over the same time interval as the coherent second pulse $a(t - T)\cos(\Omega_t t + \varphi)$ and has the same frequency, but has a different phase at any instant in time.

Figure 1.15 illustrates the difference. In the coherent case, the two pulses appear as if they were excised from the same underlying continuous, stable sinusoid; in the noncoherent case, the second pulse is not in phase with the extension of the first pulse. Another type of noncoherency arises when the starting phases φ of successive pulses are random, which occurs with some types of transmitters such as magnetrons (see Wallace et al., 2010). Because of the phase ambiguity discussed earlier, coherency also implies a system having both I and Q channels.

Another receiver requirement is that the I and Q channels have perfectly matched transfer functions over the signal bandwidth. Thus, the gain through each of the two signal paths must be identical, as must be the phase delay (electrical length of the two channels). Finally, a related requirement is that the oscillators used to demodulate the I and Q channels must be exactly in quadrature, that is, 90° out of phase with one another, not 89.9°. Of course, real receivers do not have perfectly matched channels. The effect of gain and phase imbalances will be considered in Chap. 3.

In the receiver structure shown in Fig. 1.12, the information-bearing portion of the signal is demodulated from the carrier frequency to baseband in a single mixing operation. This simple model is adequate to capture the receiver characteristics most important to radar signal processing. While convenient for analysis, radar receivers are virtually never

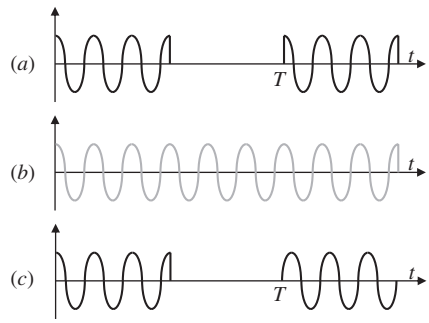

Figure 1.15 Illustration of the concept of a fixed phase reference in coherent signals. (*a*) Coherent pulse pair generated from the reference sinusoid. (*b*) Reference sinusoid. (*c*) Noncoherent pulse pair.

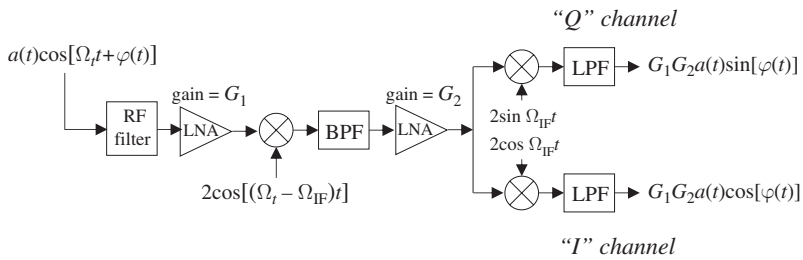

Figure 1.16 Structure of a superheterodyne radar receiver.

implemented this way in practice. One reason is that active electronic devices introduce various types of noise into their output signal, such as *shot noise* and *thermal noise* (Scheer, 1993). One noise component, known as *flicker noise* or $1/F$ *noise*, has a power spectrum that behaves approximately as F^{-1} and is therefore strongest near zero frequency. Since received radar signals are very weak, they can be corrupted by $1/F$ noise if they are translated to baseband before being amplified.

Figure 1.16 shows a more representative *superheterodyne* receiver structure. The key feature of the superheterodyne receiver is that the demodulation to baseband occurs in two or more stages. The received signal is amplified immediately upon reception using a *low-noise amplifier* (LNA). The LNA, more than any other component, determines the *noise figure* of the overall receiver. It will be seen in Sec. 2.4 that this is an important factor in determining the radar's *signal-to-noise* ratio (SNR), so good design of the LNA is important. The signal is next demodulated to an IF. The bandpass filter following the first mixer eliminates the sum frequency term, passing only the difference frequency term at the IF frequency Ω_{IF}. The RF filter eliminates any input signals at the *image frequency* $\Omega_t - 2\Omega_{IF}$; if present, these signals would generate undesired difference frequencies at the IF frequency. The signal is then amplified further. Amplification at IF is easier than at RF because of the greater percentage bandwidth of the signal and the lower cost of IF components compared to microwave components. In addition, modulation to IF rather than to baseband incurs a lower *conversion loss* (power loss in the mixer), improving the receiver sensitivity. The extra IF amplification also reduces the effect of flicker noise. Finally, the amplified signal is demodulated to baseband. Some receivers may use more than two demodulation stages so that there are two or more IF frequencies,